Abrasive Waterjet Turning 3D Jet Deflection Analysis and Process Accuracy Prediction for Al 2024 Alloy

Hande Esra Kilinc
Politecnico di Milano
Massimiliano Annoni (massimiliano.annoni@polimi.it)
Politecnico di Milano

Research Article

Keywords: abrasive waterjet turning, 3D jet deflection, jet deflection angle measurement, image processing, Al2024 alloy

Posted Date: June 22nd, 2022

DOI: https://doi.org/10.21203/rs.3.rs-1725931/v1

Abrasive Waterjet Turning 3D Jet Deflection Analysis and Process Accuracy Prediction for Al 2024 Alloy

Hande Esra Kilinc, Massimiliano Annoni

Politecnico di Milano, Dipartimento di Meccanica, Via Privata Giuseppe La Masa 1, 20156, Milano, Italia

Corresponding author Massimiliano Annoni

Contact details Postal address: Via Privata Giuseppe La Masa 1, 20156, Milano, Italia

E-mail: massimiliano.annoni@polimi.it

Phone: + 39 0223998536

Abstract

The jet deflection phenomenon is one of the main causes for the larger workpiece final diameter respect to the ideal target diameter in Abrasive Waterjet Turning (AWJT). Hence, the predetermination of the final workpiece diameter necessitates measuring the jet deflection. The aim of the present work is to develop a novel on-line measurement methodology of the 3D deflection of the jet in AWJT by the contemporary use of two cameras and a dedicated image processing routine. The selected variable machining process parameters were feed rate (V_f), depth of cut (*DOC*) and the rotational direction of the workpiece. An empirical model was developed for predicting the workpiece final diameter accuracy on Al 2024 alloy based on the jet deflection and including the effect of the jet divergence. The obtained results form the base for a new type of AWJT modelling, on-line monitoring and closed-loop control and could be a first step to make the *DOC* a handier process parameter, as it happens in standard turning.

Keywords: abrasive waterjet turning, 3D jet deflection, jet deflection angle measurement, image processing, Al2024 alloy

1. Introduction

Among the applications of AWJ machining, turning with AWJ has been a focus point for the researches thanks to its capability of machining a wide range of materials, easily adapting to their mechanical properties. The core idea of using the AWJT process as a possible replacement of the conventional turning process came from its capability to machine a various range of materials, from metal alloys to glass and ceramics, from though ones to fragile ones. Nonetheless, while conventional turning allows the users to exactly determine the workpiece final diameter based on the rigid tool location respect to the workpiece, this is still not the case with AWJT. The reason behind this issue is that the AWJ deflects when the interaction with the workpiece starts upon the first impact of the jet and from this point of view, the jet can be accepted as a soft tool.

1.1. Flow Visualization of AWJT

The original study for visualizing the AWJ flow during turning operations and also the derivation point of the present work was performed by Ansari et al. [1] to better understand the process macromechanics. During the experiments done by the pioneers [1], movies of both axial and side views were recorded. Thus, it was possible to detect the jet deflection (Fig. 1) from both X-Z and Y-Z planes. Furthermore, the study performed to profile and dress grinding wheels with AWJT by Axinte [2] confirmed that the accuracy of the turned parts with AWJ was affected by the jet trail-back and deflection.

Ansari et al. [1] revealed that as the AWJ moved towards the workpiece, the jet came in contact with the workpiece almost tangentially to its face. However, the angle between the jet and the workpiece face was not null because the jet itself has a divergence due to its original non perfectly cylindrical shape [1]. The study carried out on flow visualization of AWJT [1] led to some significant conclusions. The instantaneous diameter of the workpiece varied only in the AWJT entry stage and then the diameter reached a steady state value, which is equal to the workpiece final diameter. In addition to that, the axial deflection of the AWJ showed cyclical changing and this nature of

AWJT called for the possible existence of step formation in the removal mechanism similar to the linear cutting process [1].

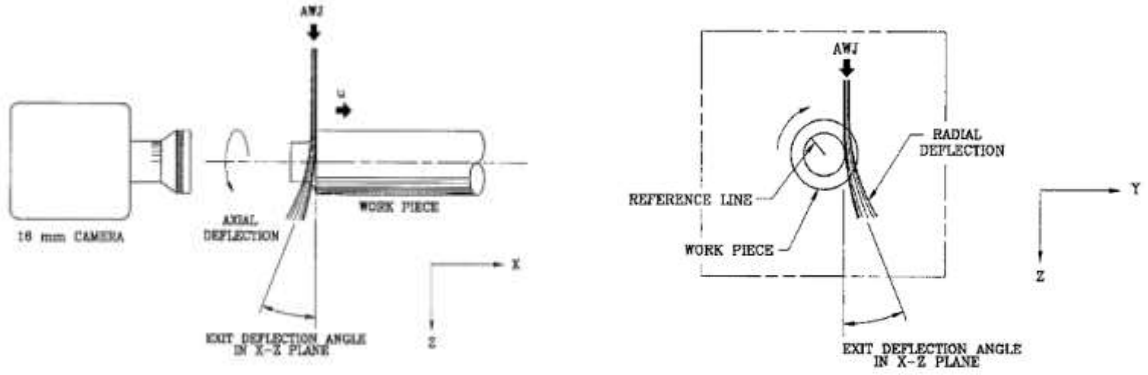

Fig. 1. Axial and side view of flow visualization experimental setup [1]

1.2. The machining process parameters

Ansari et al. [1] underlined that the typical parameters of AWJ and AWJT define the extent of the jet deflection. This statement shows the importance of the process parameters on the jet deflection. Depth of cut (*DOC*), feed rate (V_f), rotational direction of the workpiece, stand-off distance (*SOD*) are the parameters which define specifically the AWJT process beside the parameters coming from the waterjet (WJ) side [1].

Hashish and Ansari [3] conducted a research to investigate the AWJ parameters on volume removal trends in turning. The faster abrasive particles are, the higher the erosion rates for the material removal. This trend was confirmed by the authors [3]. As water pressure (P_{water}) increased, volume removal rate increased. Results regarding the abrasive mass flow rate (m_a) showed that the largest final diameter of the specimen or, in other words, the lowest volume removal rate was reached when m_a was minimum.

Manu and Babu [4] performed a study to analyze the effects of the jet impact angle (α) (Fig. 2) on material removal and surface finish with cylindrical parts turned by AWJ. The angle of the jet impacting the workpiece surface has a significant role on the resulting erosion process [4]. The workpiece diameter and the jet impact angle change continuously unless feed rate is introduced in the machining process. The material removal is influenced by this angle variation, thus the angle should be considered as an essential parameter for AWJT.

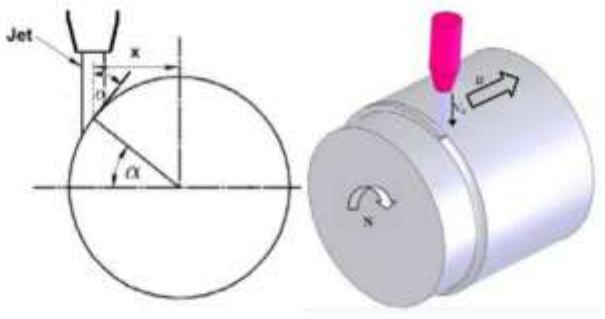

Fig. 2. Schematic representation of the impact angle in AWJT [5]

Zohoor et al. [6] performed one of the most recent and comprehensive studies to investigate the influence of machining parameters on part geometrical error (GE), which is the difference between the target diameter of the machined specimen and the real diameter measured at the end of the machining process [6]. The material used in this study [6] was AA2011-T4 aluminum alloy and the selected five variable machining parameters were P_{water}, V_f, workpiece rotational speed, m_a and DOC. The results obtained in [6] revealed that by decreasing V_f and

increasing P_{water}, it is possible to reduce GE. If V_f increases, the interaction duration between abrasive particles and workpiece surface decreases and that results in a decrease of the amount of material removed from the workpiece. The authors [6] also stated that by decreasing the *DOC* and increasing m_a, GE can be reduced. Ultimately, it was suggested to combine high m_a with low V_f to increase the amount of material that can be removed from the workpiece.

1.3. The mathematical models to predict the workpiece diameter after machining

The models developed on the workpiece final diameter prediction after machining are based on Finnie's theory of erosion [7] because the material removal mechanism during AWJ machining is the erosion done by free moving abrasive particles [5].

Hashish [8] modified the formulation in order to add the particle shape effect and also to modify the velocity exponent predicted by Finnie. The modified model of Hashish was stated as more applicable for shallow impact angles.

Manu and Babu [9] studied an erosion-based approach that considers the variations in local impact angle to predict the workpiece final diameter. Nonetheless, their model is not accurate when the V_f varies.

The model presented by the Zohourkari and Zohoor [5], applied the Hashish's erosion model. This model [5] considered the local impact angle changes, V_f variations and provided a better estimation in terms of workpiece final diameter after machining. However, the authors [5] stated that the proposed model does not consider the jet divergence so it is necessary to make further attempts to model AWJT more precisely.

What emerges from the researches up to now is the absence of a study that considers the real jet deflection phenomenon that actually occurs in the 3-dimensional space. Moreover, the impact angle depends on the workpiece diameter, has a significant role on the analytical models for the workpiece final diameter prediction and is accepted as a continuously changing parameter unless feed rate is applied to the cutting head. Studies up to now considered this impact angle only from a 2-dimensional plane. However, the jet deflects also in another plane that is perpendicular to the plane where the impact angle is usually calculated. Consequently, the part *GE* should be the result of the deflected jet in space rather than in a single plane. The objective of the present work is to develop a novel online measurement technique for the jet deflection from two perpendicular planes contemporaneously during the AWJT process by applying image processing techniques via Matlab. Then, the purpose is to attain the deflection angle in 3D by combining these two angles through a developed geometrical model, as a process performance predictor in terms of final diameter. These results could be helpful to extend the application field of AWJT through an improved modelling, monitoring and control capability.

2. Experimental setup

A lathe, which is available at the Waterjet Laboratory of Politecnico di Milano (WJ Lab) and was already used for previous AWJT researches [6] was prepared for the present study. Requirements for the lathe to accomplish the tasks of this study were checked before its positioning on the main waterjet machine frame over the water tank. The workpiece material used in the experiments was 2024 Aluminum alloy in the form of round parts, 60 mm in external diameter and 40 mm in length. Parts had a hole with an internal diameter slightly less than 22 mm to have the tight fitting condition with the shaft that holds the workpiece, whose diameter is exactly 22 mm (Fig. 3).

Fig. 3. A specimen placed on the lathe, air blowing system and black polymeric layer on the grid

A tight fitting condition was essential for this study to achieve the same speed for both the rotating shaft and the workpiece without slippage. Otherwise, the control on the rotational speed (*N)* of the workpiece would be lost and runout problems could occur. Each workpiece was placed on the shaft of the lathe for the runout verification. Runout errors up to 0.10 mm were considered acceptable and the results showed a range between 0.03 and 0.08 mm. It is worth mentioning that the diameter of the rough part plays a role on the AWJT performance, but it has been decided to keep it constant at a representative value in the frame of the present research. The motivation for this choice is to put the *DOC* role in evidence, as it is the main AWJT parameter, even more than it is in standard turning. AWJT process could improve and extend its application field if *DOC* could be treated as an independent parameter. In any case, further investigations will be devoted to involve the role of the workpiece diameter.
The composition of the alloy by percentages in weight, measured with a scanning electron microscope, is given in Table 1. The selection of this alloy was based on using a material with already known machinability and behavior for AWJ cutting. In this way, the focus of this research was directly targeted to the AWJ turning.

Table 1
The composition of Al 2024 alloy by percentages in weight

Magnesium (Mg)	Aluminum (Al)	Silicon (Si)	Titanium (Ti)	Manganese (Mn)	Iron (Fe)	Zinc (Zn)
0.94	96.79	1.38	0.15	0.39	0.14	0.21

2.1. Selected cameras and fixturing systems

Two different cameras were used to record the process from two different planes. The first camera was the Flea3 FL3 Gigabit Ethernet camera. The second one was a digital camera, Nikon D750 DSLR with the optic AF-S Nikkor 70-200 mm f/2.8G ED VR II and the TC2 Tele Converter, equivalent maximum focal length of 400 mm f/5.6. The technical specifications of the cameras are given in Table 2.

Table 2
The technical specifications of the cameras used in the experiments [11]

	Flea3 FL3 Gigabit Ethernet Camera	*Nikon D750 DSLR Digital Camera*
Resolution	1288*964	6032*4032
Frame Rate (fps)	30	25
Megapixels (MP)	1.3	24.3
Sensor Type	CCD	CMOS
Camera Sensor	Monochrome	RGB

A special fixturing system and casing (Fig. 4) were needed for the Flea3 FL3 Gigabit Ethernet camera to preserve the focal distance between the camera and the machining region. The WJ head could move out from the camera and the image would have gone immediately out of focus in case there would not be such a system. The whole system was designed and manufactured by considering some technical aspects as the compactness, the ease of

assembly and the waterproofness. The focal distance issue was not present for the D750 digital camera since the WJ head was moving along a plane perpendicular to the D750 optical axis, thus avoiding the possibility to go out of focus. Moreover, there was no need to move the camera. For this reason, it was decided to locate the digital camera far enough from the machining zone.

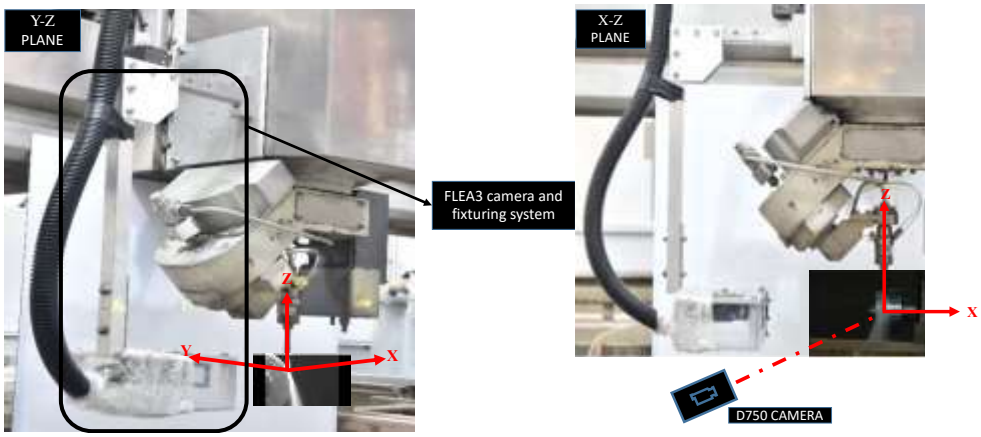

Fig 4. The experimental setup with its reference axes

A 20 m RJ45 category Cat7 Ethernet cable was used to connect the Flea 3 camera to a PC where its software was installed. The Ethernet cable together with the power cable of the camera and a pressurized air inlet pipe, which was needed to repel the water that might enter from the square hole in the camera casing, were brought together. After that, this combination of 2 cables and the air pipe were passed through the rail of the AWJ cutting head to prevent any possible cable-water interaction. Once the cables reached the main body of the AWJ cutting head, they were put into a larger diameter pipe connected to the camera casing (black pipe in Fig. 4).

There were also additional modifications to improve the experimental conditions. The lathe frame staying inside the camera view was covered with a black polymeric layer to increase the contrast between jet-workpiece interaction and background (Fig. 3, left). A pressurized air blowing system was developed by creating a specific manifold with 3 nozzles and a main connecting channel for the air pipe (Fig. 3, centre). Aim of this system was to prevent the possible water waves that might come from below during the machining process. The upper surface of the water pool grids that carry the lathe and other equipment were covered with a black polymeric layer for the already described purpose (Fig. 3, bottom).

The WJ/AWJ machine used in experiments was an Intermac Primus 322, equipped with a BHDT Ecotron 4037 pump that are at the WJ Lab of Politecnico di Milano. The Intermac Primus 322 is equipped with a CAD/CAM software (iCam) for programming the manufacturing process. The machining process for the experiments were prepared in a way that when the jet is turned on, it has a linear approaching distance of 3 mm to the workpiece and then it starts to machine a length of 15 mm along the workpiece axis. The trajectory prepared in iCam was the same for each experimental run. It was decided to use initially one side of the workpiece and then machine the other side by removing and replacing the part. In fact, the workpiece was 40 mm in length and the machining stroke was only 15 mm. Hence, one workpiece could be used for two experimental runs.

2.2. Positional Referencing Methodology

The machining process reference point had to be systematically determined by adjusting the position of the jet, taking into account the dimensions and shape of the workpiece. To set the *DOC*, the cutting head was radially moved from the workpiece center to the position where the jet was tangent to the workpiece surface (Fig. 5). Then, the cutting head was moved inward of a value equal to the *DOC*. To set the *SOD*, the point where the jet touched the outer surface of the workpiece after setting the *DOC* was found. The *SOD* was defined as the distance along the Z-axis between that point and the tip of focusing tube along its axis. The impact point of the jet on the workpiece was set as the origin of the reference system used in this paper (Fig. 4).

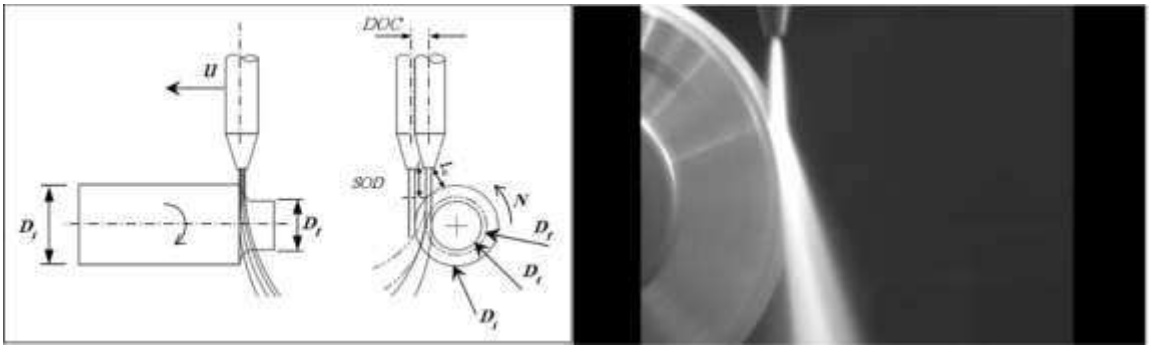

Fig 5. Definition of *DOC* and *SOD* (left) [6] with a frame from the Y-Z plane during machining (right)

While the Flea3 FL3 Gigabit Ethernet camera, the one mounted in the casing (Fig. 4) and moving with the AWJ cutting head, was used for recording the process in the Y-Z plane (Fig.4), the Nikon D750 DSLR was used for recording the process in the X-Z plane. The camera on the Y-Z plane was positioned in a way that the lens was aligned with the tip of the focusing tube thanks to adaptiveness feature of the fixturing system. When the position of the camera was assigned, the best focal point of the camera was detected and then the camera casing was closed. The other camera framing the X-Z plane was placed on a tripod close to catcher tank in line with the focusing tube. After that, it was zoomed to the machining zone.

During the experiments, the D750 digital camera was triggered manually and the FLEA3 Gigabit Ethernet camera was triggered via software when the jet was turned on. They were stopped when the jet completed the machining length and started to move along the exiting path. The two cameras had different frame rates and they were not synchronous since they were triggered manually.

2.3. Experimental design

The ranges of the selected factors *DOC*, V_f and rotational direction of the workpiece were identified based on the preliminary experiments and the literature survey. Afterwards, the selected parameters were used to create a Central Composite Design (CCD) experimental plan. The CCD is an effective design able to handle linear, quadratic and interaction terms in statistical modeling of processes [10]. The CCD created for this study considered V_f and *DOC* as the continuous factors with 5 levels. The continuous factors of the AWJT experimental campaign with their levels are shown in Table 3. The rotational direction of the workpiece was the categorical factor with 2 levels which are clockwise (CW) and counterclockwise (CCW) (Table 3). The total number of experiments is 24 with 8 replicates in the center point (Fig. 6).

Table 3
The CCD design factors with their levels

Process Parameter	Symbol	Unit	*Level 1* Lower axial point	*Level 2* Lower corner point	*Level 3* Center point	*Level 4* Higher corner point	*Level 5* Higher axial point
Depth of cut	*DOC*	mm	2	2.3	3	3.7	4
Feed rate	V_f	mm/min	15	17.2	22.5	27.8	30
Rotational direction	-	-			CW/CCW		

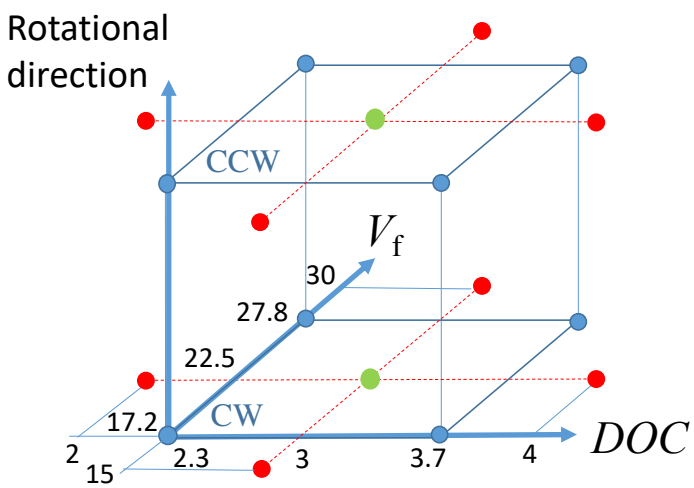

Fig 6. Experimental design (CCD) representation. Experimental conditions are represented with dots. All conditions were replicated one time apart from center points (green) that were replicated 4 times each

The machining process parameters, which were kept constant during the experiments, are listed in Table 4.

Table 4
The constant process parameters of the experiments with their values

Process Parameter	Symbol	Unit	Value
Abrasive mass flow rate	m_a	g/min	350
Water pressure	P_{water}	MPa	380
Rotational speed	N	rpm	200
Stand-off distance	SOD	mm	10
Abrasive type	-	-	Garnet
Abrasive particle size	#	-	80
Focusing tube diameter	d_f	mm	1.02
Primary orifice diameter	d_0	mm	0.33

It was decided to keep m_a and P_{water} constant at their maximum value since most of the AWJ machining processes are performed by using the highest cutting capability available. For the same reason, d_f and d_0 were selected as the best performing ones for the used machine and pump. The used abrasive type and mesh are a waterjet cutting standard. Rotational speed N and SOD have been kept constant as their role is not so influential according to literature and preliminary experiments.

3. Measurements

Image processing can be considered as a sort of signal processing taking the digital image as an input of the system and giving information or specific parameters as an output to the user. The principal aim to use the image processing to measure the deflection angle is that each recorded video can be elaborated to extract its frames. Following that, the deflection angle measurement can be performed through the analysis of all the process frames. Thus, the deflection angle modifications during the process can be assessed. Each digital image extracted from the video has a finite number of pixels and each one has a particular location and a value. The binary images contain only two pixel elements that are “0” and “1”. “0” refers to white and “1” refers to black. The algorithm of the code developed is based on this information.

3.1. The deflection angle measurement on the Y-Z plane

The machining process recording for the Y-Z plane was performed with the Flea3 FL3 Gigabit Ethernet camera.

The videos were acquired in gray scale and with 30 frames per second. As indicated before, since the camera triggering was done manually via software, the total number of obtained frames was different for each video.

The recorded video of each experimental run was read by Matlab. The total number of frames was counted and saved. Further, the video frames were extracted and saved. A single frame extracted from the machining process video on the Y-Z plane is shown in Figure 4, image 1. The optimized binarization threshold value (the same for all the frames) was found and set to convert each frame to binarized form to detect the edges of the jet. Following this, the image changed as shown in Figure 7, image 2.

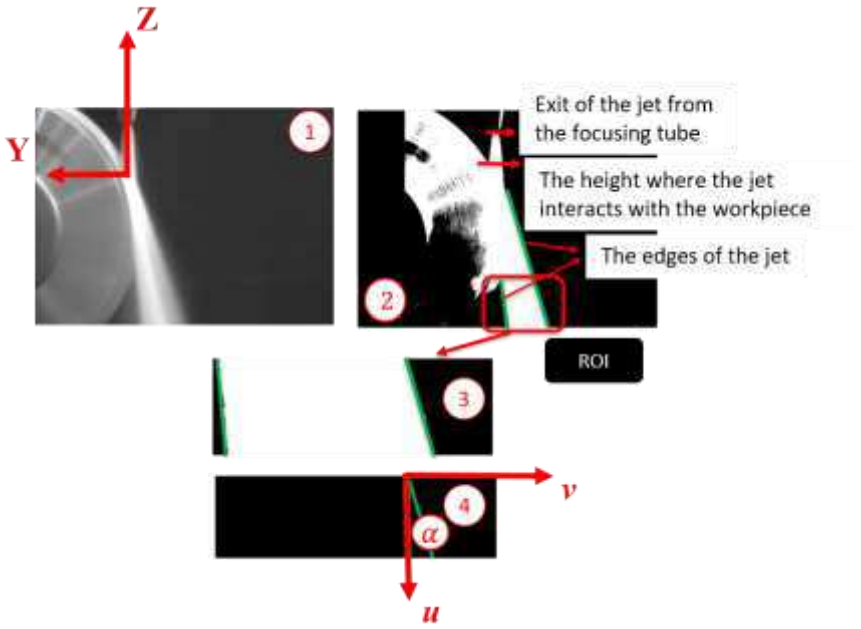

Fig. 7. The deflection angle measurement steps on the Y-Z plane

All the video frames were checked to decide which points to take as a reference to measure the deflection angle. Then, it was found out that the green edge indicated on the left (Fig. 7, image 2) was not always showing a straight profile due to the jet-workpiece interaction. On the other side, the green edge that is on the right (Fig. 7, image 2) was changing with a linear profile almost for each frame and it was more robust to detect. In the beginning, it was aimed to catch the axis of jet and take it as reference but since the green edge on left was generally distorted, it was understood that catching a defined axis of the jet was not feasible.

A specific narrowed region of interest (ROI) was identified to focus on the red rectangle in Fig. 7, image 2. Furthermore, the image 2 was cropped to the image 3. The rest of the analysis continued in this ROI for each frame. By starting to analyze the image 3 in Fig. 7 from the right upper corner of the image, the transition pixels from black to white were detected and their coordinates were saved in a matrix called “edge”. In this way, the green edge on the right in image 3 could be extracted. Polynomial line fitting was applied to the points in the “edge” matrix. After that, Matlab returned a linear equation in the form of $v = au + b$ with its coefficients a and b. Knowing that the slope of the line is equal to a, the angle indicated with α in Fig. 7 image 4 could be calculated by using the Eq. 1.

$$\alpha = \arctan(a) \tag{1}$$

The calculated deflection angle was converted from radians to degrees. These steps were repeated in a loop to perform the measurement for each single frame to obtain a graph of the deflection angle vs. the frame number. The graph obtained is shown in Fig. 8.

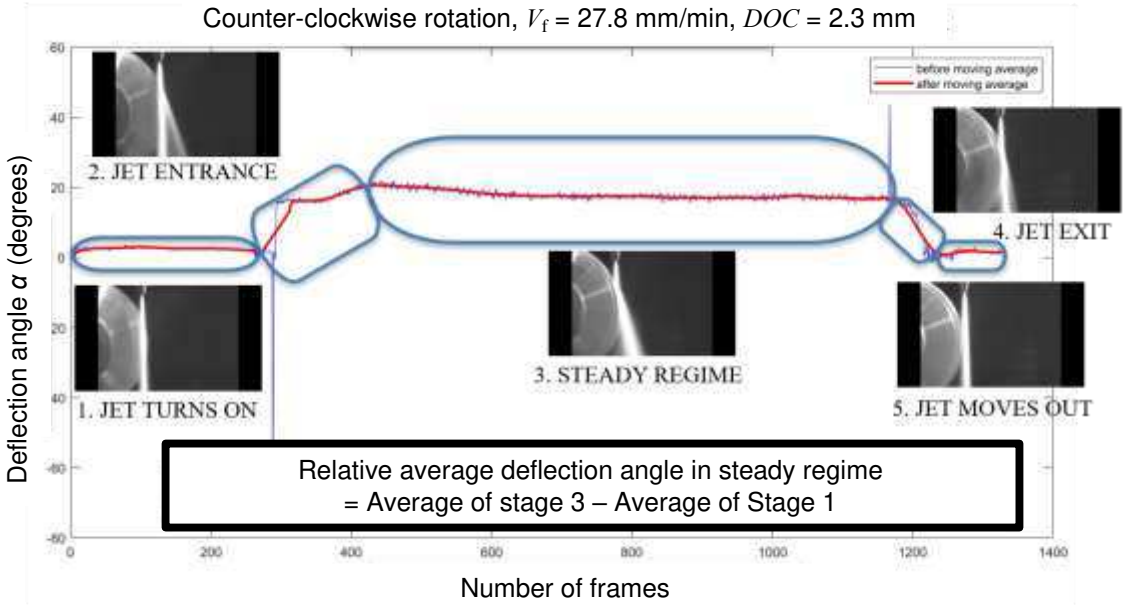

Fig. 8. The relative average deflection angle in steady regime vs the number of frames with the defined stages of the machining process on the Y-Z plane

The moving average filter was applied by creating a series of averages. A subset of 50 data points was taken to remove the peaks from the graph. In fact, there were some peaks detected on the graph before applying the filter. They were checked by detecting the number of the frame where they took place and then by checking the first saved version of the frame to understand the reason. In most of the cases, it was found out that peaks occurred due to instantaneous water splashes.

Furthermore, it was observed that the jet itself has already an angle when moving along the approaching length of the trajectory before starting the machining process. This finding approved the jet natural divergence which was also mentioned by Ansari and Hashish [1]. By taking the shape of the graph in Fig. 8 into consideration, it is possible to say that, besides when the jet turns on and moves out, there are 3 main process stages. These stages are named as the jet entrance, the steady regime and the jet exit. The jet entrance stage defines the interval which starts with the first impact of the jet until it reaches the steady regime. In the steady regime, the jet demonstrates small changes in terms of deflection angle. The jet exit refers to the last part of the machining length. In this stage, the jet starts to turn to its original form. The explained stages are shown in Fig. 8.

Considering that the two cameras were not synchronous and the number of frames for each run was different, a method had to be developed to define a deflection angle that is representative for the machining process in certain conditions. It was decided to take the average value of the steady regime and name it as “average deflection angle in steady regime”. However, as already mentioned, it was also realized that the jet has already an initial angle before the machining starts. Thus, the average value of the angle when the jet turns on before the machining starts had to be subtracted from the average deflection angle in steady regime. The obtained value after subtracting the initial angle of the jet is the resulting deflection angle and it was called “relative average deflection angle in steady regime”.
The procedure for calculating the average deflection angle in the steady regime had to be defined clearly to be robust to the variability of the graphs obtained for the various experimental runs. After examining the obtained graphs, it was decided to give the user the possibility to select the first and the last point of the steady regime by considering that the first point has to be in the region where the deflection angle variations start to be small and the last point has to be in the region where the deflection angle starts to decrease without increasing again. After that, Matlab gives the average value between those selected two points. This last step was decided to be repeated 3 times to consider the measurement error due to the user. Then, the final relative deflection angle was accepted as the average value of those 3 measurements.

3.2. The deflection angle measurement on the X-Z plane

The machining process recording from the X-Z plane was performed with the digital camera. The videos were acquired in RGB format and with 25 frames per second. The algorithm of the Matlab code to calculate the deflection angle on the X-Z plane was developed by modifying the code developed for the Y-Z plane. The frames of the videos were extracted as RGB images and they were converted to the grayscale. As done for the YZ plane, all frames of the video of the X-Z plane were checked to decide which points to take as a reference to measure the deflection angle. Then, it was found out that the edge, which was indicated with the green line on the right of Fig. 9, image 2, was not always showing a straight profile and its form was not due to the jet deflection. Hence, it would have been misleading to select it. On the contrary, the edge that is showed with the green line on the left of Fig. 9, image 2 was changing with a linear profile almost for each frame and it was the edge that needed to be considered as the deflection edge. The ROI was analyzed starting from the left upper corner of the image this time, differently from the algorithm of the Y-Z plane, to detect the transition pixels of the green edge on left shown in Fig. 9, image 3.

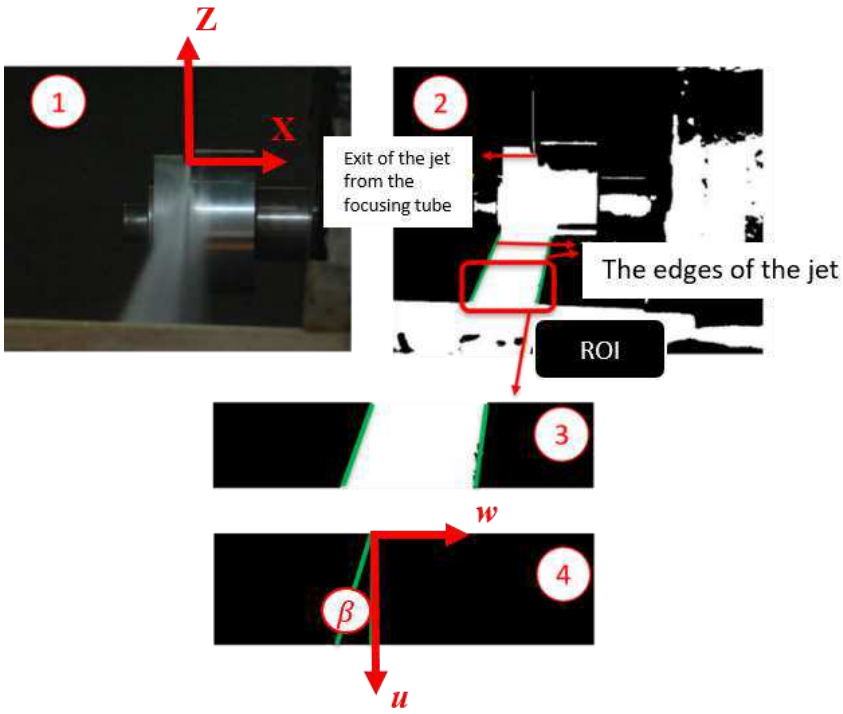

Fig. 9. The deflection angle measurement steps on the X-Z plane

By applying the same methodology described in Section 3.1, the deflection angle on the X-Z plane was calculated by the Eq. 2

$$\beta = \arctan(c) \quad (2)$$

where c is the slope of the line $w = cu + d$.
The graph obtained for the deflection angle measured with respect to the number of frames on the X-Z plane is shown in Fig. 10.

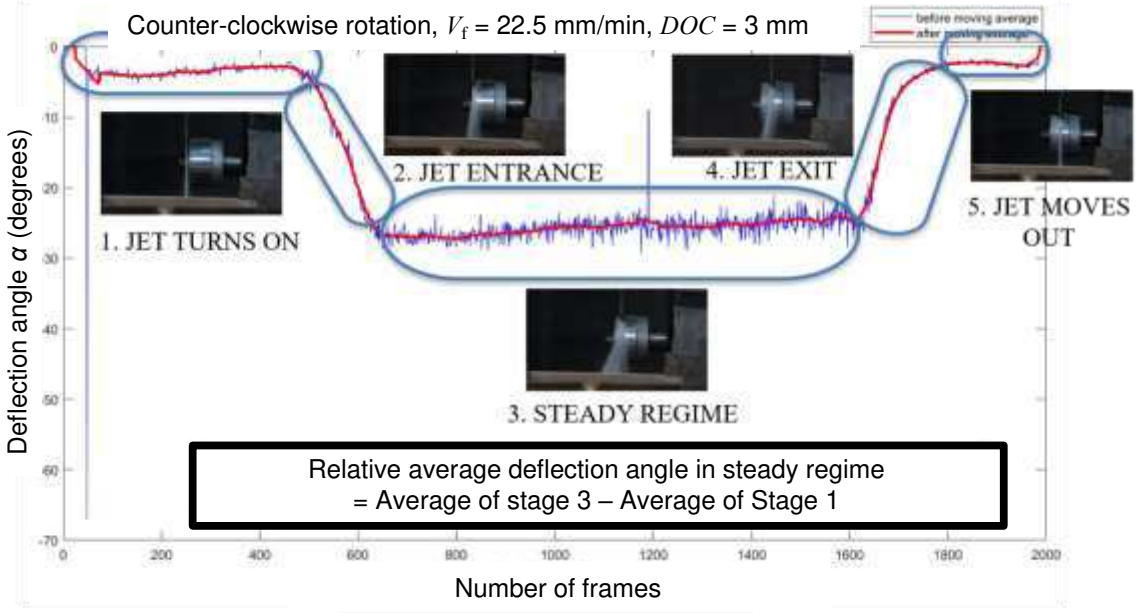

Fig. 10. The relative average deflection angle in steady regime vs the number of frames with the defined stages of the machining process on the X-Z plane

The reason of the negative value of the measured deflection angle was that the deflection angle measured in the Y-Z plane which was in *CCW* direction was accepted as positive in the code (Fig. 11). Thus, the angle formed in the X-Z plane which was *CW* became negative to be consistent. This reference system was used for the model to obtain a deflection angle in space. The stages of the machining process defined for the Y-Z plane were valid also for these measurements. For this reason, the same methodology to define the deflection angle explained in Section 3.1 was applied here too.

3.3. The geometrical model developed to obtain the deflection angle in space

The two deflection angles measured in two different planes for each experimental run needed to be combined to obtain a deflection angle in space. The 3-dimensional angle was obtained by means of the developed geometrical model. In Figure 11, α is the deflection angle measured on the Y-Z plane. The blue circle in the origin is the impact point of the jet on the workpiece. The stand-off distance is indicated as *SOD* (Fig. 11). This distance was equal to 10 mm and it was kept constant during all the experiments (Table 4). $\overrightarrow{Va}$ is the projection of the jet velocity vector measured on the Y-Z plane after the impact of the jet on the workpiece. Vector $\vec{a}$ is the Z component of the jet velocity. The *CCW* angle was accepted as positive respect to the vertical axis.
For the sake of simplicity, the notation X+ and X- has been used in the following to indicate respectively the positive and the negative directions of the X axis. The same has been done for Y and Z.

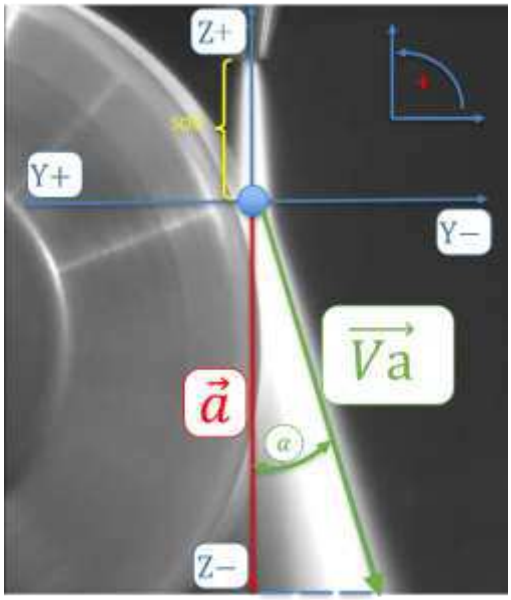

Fig. 11. The drawing of the deflection angle measured on the Y-Z plane (this view corresponds to view 1 in Fig. 7; α is the same as in Fig. 7)

In Figure 12, β is the deflection angle measured on the X-Z plane. The blue circle in the origin is the impact point of the jet on the workpiece. The *SOD* was equal to 10 mm and, as said before, it was kept constant during the machining processes (Table 4). $\overrightarrow{V\text{b}}$ is the projection of the jet velocity vector measured on the X-Z plane after the impact of the jet on the workpiece. Vector $\vec{a}$ is the Z component of the jet velocity. The jet velocity vectors $\overrightarrow{V\text{a}}$ and $\overrightarrow{V\text{b}}$ are inclined respect to the vertical direction of respectively the relative average deflection angle in steady regime α and β.

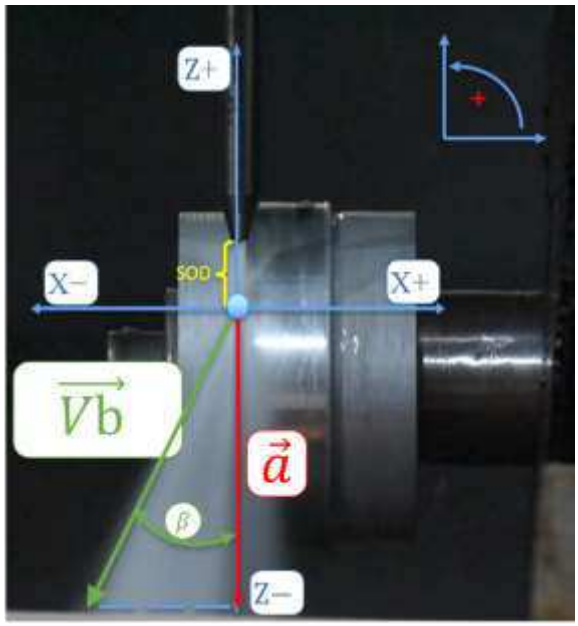

Fig. 12. The drawing of the deflection angle measured on the X-Z plane

$$|\overrightarrow{V\text{b}}| = \frac{|\vec{a}|}{cos\beta} \quad (3)$$

$$|\overrightarrow{V\text{a}}| = \frac{|\vec{a}|}{cos\alpha} \quad (4)$$

Versors $\vec{\imath}, \vec{\jmath}, \vec{k}$ are introducd as indicated in Fig. 13. The components of the vectors $\overrightarrow{V\text{a}}$ and $\overrightarrow{V\text{b}}$ become:

$$\overrightarrow{V\mathrm{b}_{X-}} = (\frac{|\vec{a}|}{cos\beta} sin\beta\ )\vec{\imath} \quad (5)$$

$$\overrightarrow{V\mathrm{b}_{Z-}} = |\vec{a}|\overrightarrow{k} \quad (6)$$

$$\overrightarrow{V\mathrm{a}_{Y-}} = (\frac{|\vec{a}|}{cos\alpha} sin\alpha)\vec{\jmath} \quad (7)$$

$$\overrightarrow{V\mathrm{a}_{Z-}} = |\vec{a}|\overrightarrow{k} \quad (8)$$

Therefore,

$$\overrightarrow{V\mathrm{b}} = (|\vec{a}|tan\beta)\vec{\imath} + |\vec{a}|\overrightarrow{k} \quad (9)$$

$$\overrightarrow{V\mathrm{a}} = (|\vec{a}|tan\alpha)\vec{\jmath} + |\vec{a}|\overrightarrow{k} \quad (10)$$

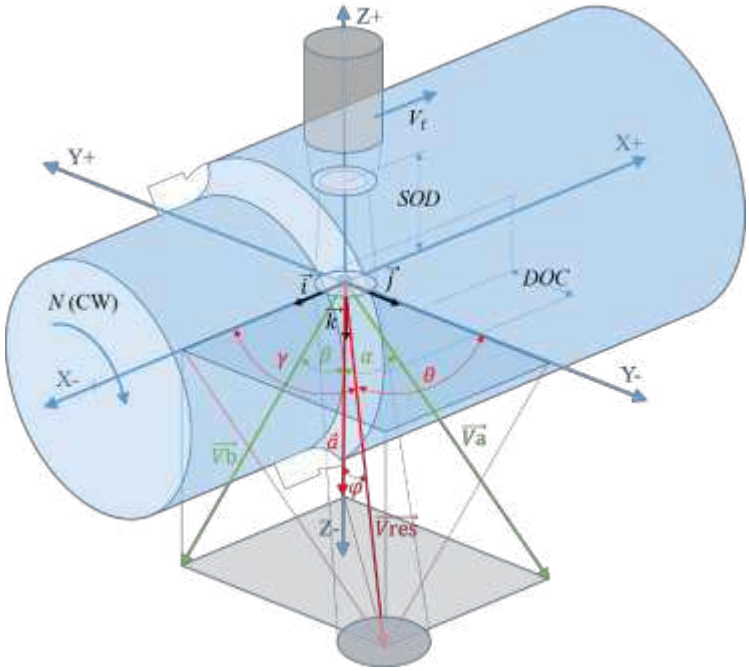

Fig. 13. 3D representation of relevant vectors, angles and process parameters

The vector $\overrightarrow{V\mathrm{res}}$ represents the measured jet velocity vector in space and can be obtained as:

$$\overrightarrow{V\mathrm{res}} = (|\vec{a}|tan\beta)\vec{\imath} + (|\vec{a}|tan\alpha)\vec{\jmath} + |\vec{a}|\overrightarrow{k} \quad (11)$$

$\overrightarrow{V\mathrm{res,norm}}$ is obtained by normalizing $\overrightarrow{V\mathrm{res}}$ with respect to $|\vec{a}|$:

$$\overrightarrow{V\mathrm{res,norm}} = \frac{\overrightarrow{V\mathrm{res}}}{|\vec{a}|} = tan\beta\ \vec{\imath} + tan\alpha\ \vec{\jmath} + \overrightarrow{k} \quad (12)$$

By using the analytic geometry, the direction cosines of the vector $\overrightarrow{V\mathrm{res,norm}}$, which are the cosines of the angles between the vector $\overrightarrow{V\mathrm{res,norm}}$ and the three coordinate axes, can be written.

γ, the angle between the X- axis and $\overrightarrow{V\mathrm{res,norm}}$ is:

$$\gamma = cos^{-1}(\frac{tan\beta}{\overrightarrow{V\mathrm{res,norm}}}) \quad (13)$$

θ, the angle between Y- axis and $\overrightarrow{V\mathrm{res,norm}}$ is:

$$\theta = cos^{-1}(\frac{tan\alpha}{|\overrightarrow{V\mathrm{res,norm}}|}) \quad (14)$$

φ, the angle between Z- axis and $\overrightarrow{V\text{res}, \text{norm}}$ is:

$$\varphi = cos^{-1}\left(\frac{1}{\left|\overrightarrow{V\text{res},\text{norm}}\right|}\right) \quad (15)$$

Where $\left|\overrightarrow{V\text{res}, \text{norm}}\right|$ is:

$$\left|\overrightarrow{V\text{res}, \text{norm}}\right| = \sqrt{(tan\alpha)^2 + (tan\beta)^2 + 1^2} \quad (16)$$

The relative average deflection angle in steady regime in space φ is the angle between $\overrightarrow{V\text{res}, \text{norm}}$ and the Z- axis (Fig. 13). The developed geometrical model was applied to each experimental run.

3.4. The DOC error measurement

The final diameter of the workpiece measured after the machining process was different than the ideal target diameter of the workpiece, as expected in AWJT. The depth of cut error in percentage was measured to investigate the machining process performance. Ultimately, the purpose was to correlate the jet deflection angle measured in space with the depth of cut error in percentage. The workpiece diameter measurements were done on a Zeiss Prismo Navigator Coordinate Measuring machine (CMM) equipped with a VAST sensor and a 5 mm ruby probe. According to the specifications provided by Zeiss, the CMM has a length measurement error of 0.5 + L/500 µm. The percentage depth of cut error was found according to the following equations. $DOC\text{meas}$ in Eq. 17 is the measured value of *DOC*.

$$DOC\text{meas} = \frac{\text{Initial diameter of the workpiece} - \text{Final diameter of the workpiece}}{2} \quad (17)$$

The error on the DOC ($DOC\text{err}$) is calculated according to the Eq. 18. $DOC\text{err}$ is always positive since the jet always removes less material than expected as it is not straight during the turning operations, but it is deflected by the interaction with the workpiece. This is a natural effect in AWJT and this paper aims at predicting it.

$$DOC\text{err} = \text{Nominal value of } DOC - DOC\text{meas} \quad (18)$$

The percentage depth of cut error ($DOC\text{err}\%$) is finally obtained from Eq. 19.

$$DOC\text{err}\% = \left(\frac{DOC\text{err}}{\text{Nominal value of DOC}}\right) \times 100 \quad (19)$$

4. Results and Discussion

4.1 Results of the design of experiments (DOE) analysis

The statistical analyses were performed by considering the relative average deflection angle in steady regime in space φ and the percentage depth of cut error $DOC\text{err}\%$ as two separate responses.

The *DOC* is the main effect on φ (Fig. 14, left). It is possible to conclude that by considering α = 0.05 (95% confidence level), all the factors are significant. Furthermore, the value of R-sq(adj) is 93.01%, which points out the appropriateness of the model. The of the lack of fit p-value is 0.843. The null-hypothesis of the lack-of-fit test is that the model correctly specifies the relationship between the response and the factors. If the p-value of the lack of fit is bigger than the significance level, it means that lack of fit is not statistically significant. Hence, no lack of fit is detected. Thus, the model correctly specifies the relationship between the response and the factors. The normality hypothesis cannot be rejected since its p-value was equal to 0.254. All the normalized residuals are within the interval [-3;+3], which tells that there are no outliers. From the obtained contour plots (Fig. 15, left), it is observed that the high values of *DOC* combined with high values of V_f result in higher values of φ.

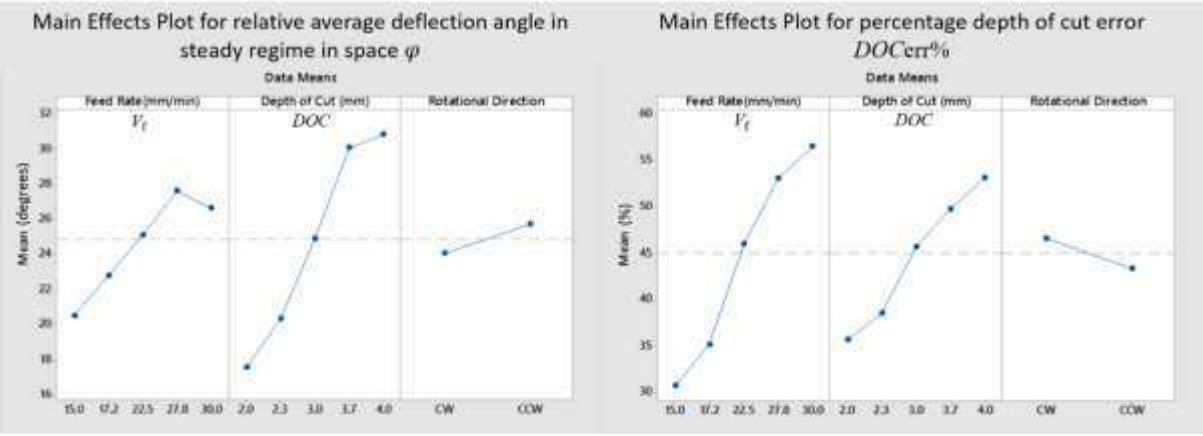

Fig. 14. The main effect plot for the relative average deflection angle in steady regime in space φ (left) and percentage depth of cut error $DOCerr\%$ (right)

V_f is the main effect on DOCerr% (Fig. 14, right). All the factors and the square terms of factors V_f and DOC were significant but not the two-way interactions. The R-sq(adj) is 99.27% and this value provides a high strength to the model. The model correctly specified the relationship between the depth of cut error and the factors since the p-value of the lack of fit was equal to 0.445. The hypothesis of normality cannot be rejected as the p-value is equal to 0.343. From the obtained contour plots (Fig. 15, right), it is observed that the high values of DOC combined with high values of V_f result in higher values of DOCerr%, at it happens for φ.

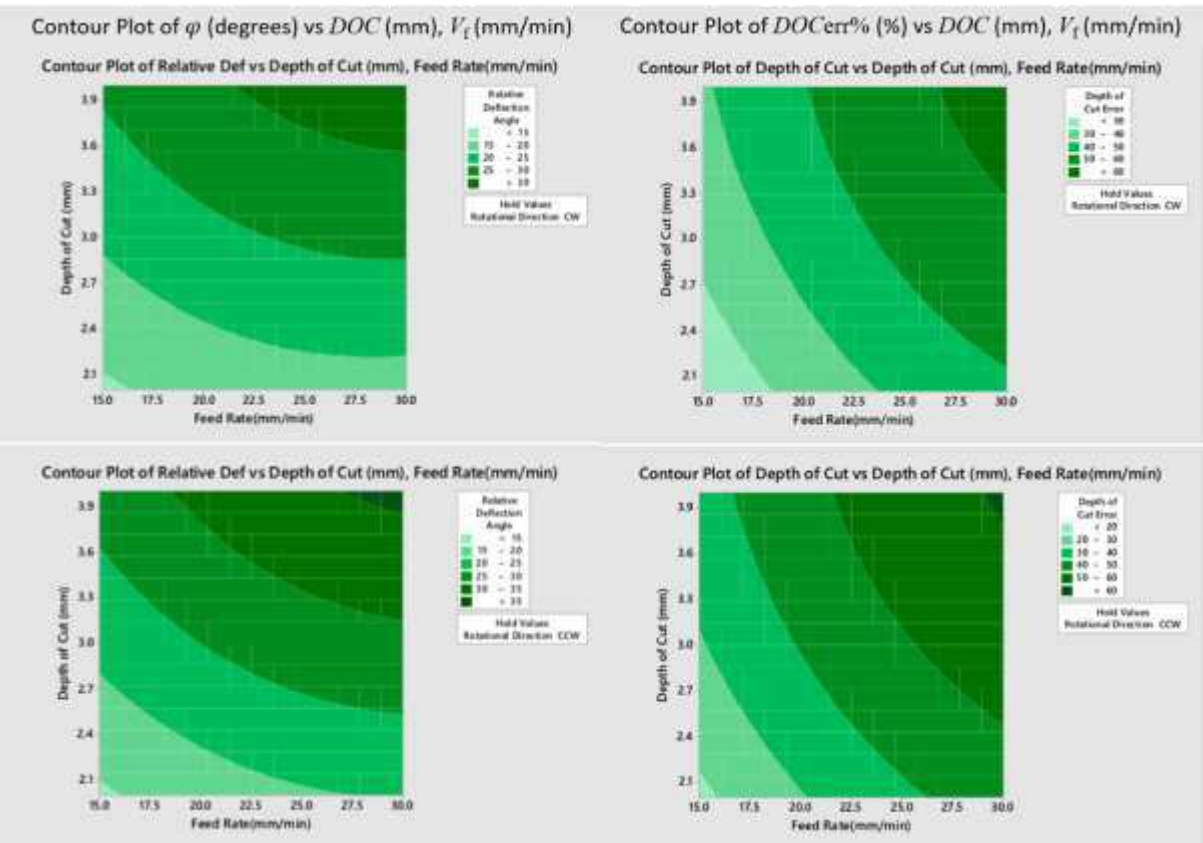

Fig. 15. Contour plot for the relative average deflection angle in steady regime in space φ (left) and percentage depth of cut error $DOCerr\%$ (right) (CW rotational direction (up) and CCW rotational direction (down))

4.2 The regression model for the prediction of the percentage depth of cut error

After completing the CCD analyses, the correlation between the two responses was checked. A Pearson

correlation coefficient equal to 1 defines the perfectly linear relationship between the terms. In the present work, with a Pearson correlation coefficient of 0.773, it is possible to say that there is a moderate correlation between DOCerr% and φ. According to the correlation analysis results, a regression analysis between DOCerr% and φ was performed. The regression results are given in Table 5 and in Fig. 16. The regression analysis is based on the principle that the jet deflection in space causes the depth of cut error. Hence, φ is accepted as the predictor of DOCerr%.

Table 5
Regression Analysis: $DOCerr\%$ versus φ. Analysis of Variance

Source	DF	Adj SS	Adj MS	F-Value	P-Value
Regression	1	1184.3	1184.27	32.67	0.000
φ	1	1184.3	1184.27	32.67	0.000
Error	22	797.5	36.25		
Total	23	1981.8			

Model Summary

S	R-sq	R-sq(adj)	R-sq(pred)
6.02079	59.76%	57.93%	52.65%

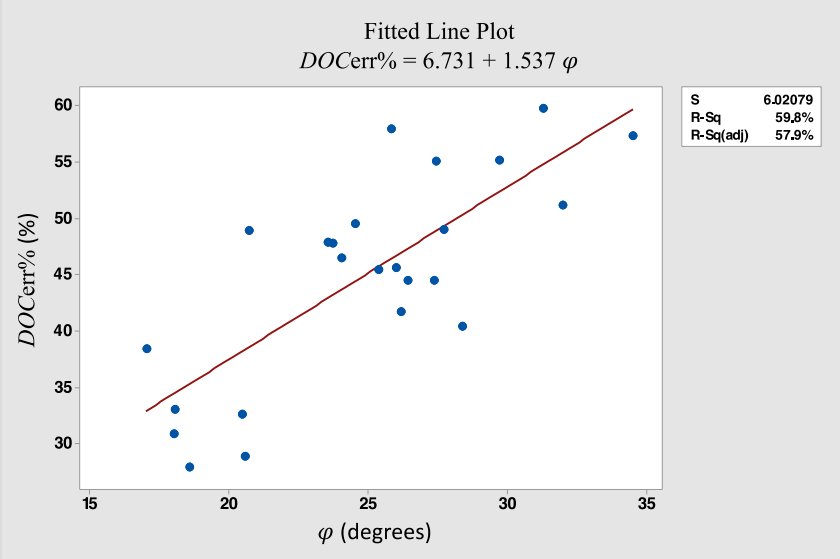

Fig. 16. Fitted Line Plot of the Regression Model

The performed regression analysis established that the model is significant, as indicated by the p-value. φ statistically can predict DOCerr%. φ is accounted for the 59.76% of the explained variability in DOCerr%. The obtained regression equation is reported as Eq. 20, where φ is in degrees.

$$DOC\text{err}\% = 6.731 + 1.537\ \varphi \tag{20}$$

After obtaining the Eq. 20, it was used to predict DOC values starting from the φ values available from the experiments. The error between the measured and the predicted values of DOCerr% was calculated. After finding this error for each experimental run, it was averaged. The final average error between finding DOCerr% by measurements and by using the regression model is 11.67%. In other words, it is concluded that the obtained regression model can predict the DOCerr% with an average error of 11.67%.

The fact that DOCerr% can be predicted simply using φ proves that φ is an index of the AWJT removal capability, as it was an energy indicator, irrespectively of the process parameters that determine that energy. It is worth

mentioning that being able to predict $DOC\text{err}\%$ through on-line measurements of φ means being able to compensate for workpiece diameter errors by moving the cutting head inward accordingly.

5. Conclusions

In the present study, a novel 3D measurement method for the jet deflection phenomenon during the AWJT process of Al 2024 alloy cylindrical rods was developed. Moreover, an empirical model to predict the depth of cut error was presented. The deflection angle measured against the number of frames was plotted to evaluate the variation of the deflection angle through the machining process. It was inspected from the obtained graphs that the jet itself has already an angle due to the jet natural divergence when it moves along the approaching length of the machining trajectory, before the machining starts. Also, the shape of the graph indicates that there are 3 main stages in the AWJT process as the jet entrance, the steady regime and the jet exit. Once the two relative average deflection angles in steady regime from two different planes were measured, a geometrical model was developed to combine them to obtain the so called relative average deflection angle in steady regime in space φ, representing the jet deflection in 3D.

A regression analysis between φ and the percentage depth of cut error $DOC\text{err}\%$ was performed. The regression analysis was done based on the principle that jet deflection in space causes the *DOC* error. Hence, φ was accepted as the predictor of the depth of cut error. This analysis allowed to obtain a model to predict the value of $DOC\text{err}\%$ from φ measurements. It was concluded that the model obtained could predict the *DOC* error value within an average error of 11.67%.

Some further activities have been already identified to improve the current model. The first one is to extend the model to involve the role of the workpiece initial diameter. When the diameter of the rough part is increased, more material should be removed by the jet to achieve the same nominal *DOC*. At the same time, the impact angle changes and modifies the jet removal capability. This fact leads to phenomena that are worth to be investigated to make the model more general. As a further development of this work, the cameras used in the monitoring operations can be synchronized by using the same frame rates and automatic triggering system. Then, the developed geometrical model can be applied to find the 3D relative deflection angle not as an averaged value but as an instantaneous one. If these steps can be achieved, the developed approach could be a useful tool for an on-line monitoring system and a closed loop control algorithm for an AWJT dedicated machine. The approach and modelling effort presented in this paper will be useful to be the empirical part of more complex models, capable for example to predict the jet deflection through the fluid-dynamic interaction of the jet with the workpiece or to validate them.

6. Declarations

6.1 Ethics approval and consent to participate

We have read the Springer journal policies on author responsibilities and submit this manuscript in accordance with those policies.

6.2 Consent for publication

We confirm that we understand journal Experiments in Fluids is a transformative journal. When research is accepted for publication, there is a choice to publish using either immediate gold open access or the traditional publishing route.

6.3 Availability of data and materials

Data and materials are available.

6.1 Competing interests

The authors have no relevant financial or non-financial interests to disclose.

6.1 Funding

Not applicable

6.2 Authors' contributions

H.E. Kilinc carried out the experimental work under the direct guidance of M. Annoni and wrote the main manuscript draft. M. Annoni designed and implemented figures 6 and 13 and reviewed the manuscript.

6.3 Acknowledgements
The authors wish to thank Dr. Francesco Viganò and Eng. Francesco Cacciatore for supporting and guiding the experimental part of this study with their knowledge and experience.

7. References

[1] A. I. Ansari, M. Hashish, and M. M. Ohadi, "Flow visualization study of the macromechanics of abrasive-waterjet turning," *Exp. Mech.*, vol. 32, no. 4, pp. 358–364, 1992.
[2] D. A. Axinte, J. P. Stepanian, M. C. Kong, and J. McGourlay, "Abrasive waterjet turning-An efficient method to profile and dress grinding wheels," *Int. J. Mach. Tools Manuf.*, vol. 49, no. 3–4, pp. 351–356, 2009.
[3] A. I. Ansari and M. Hashish, "Effect of abrasive waterjet parameters on volume removal trends in turning," *J. Eng. Ind.*, vol. 117, no. 4, pp. 475–484, 1995.
[4] R. Manu and N. R. Babu, "Influence of jet impact angle on part geometry in abrasive waterjet turning of aluminium alloys," *Int. J. Mach. Mach. Mater.*, vol. 3, no. 1/2, p. 120, 2008.
[5] Zohourkari I and Zohoor M. Mathematical modeling of abrasive waterjet turning of ductile materials. In: ASME 2010 10th biennial conference on engineering systems design and analysis (ESDA2010), Istanbul, Turkey, 12– 14 July 2010. New York: ASME.
[6] M. Zohoor, I. Zohourkari, F. Cacciatore, and M. Annoni, "Influence of machining parameters on part geometrical error in abrasive waterjet offset-mode turning," *Proc. Inst. Mech. Eng. Part B J. Eng. Manuf.*, vol. 229, no. 12, pp. 2125–2133, 2015.
[7] G. Yadav, S. Tiwari, A. Rajput, R. Jatola, M. L. Jain, and A. Professor, "A Review: Erosion Wear Models," *Int. Conf. Emerg. Trends Mech. Eng. "ICETME – 27-28 may 2016,"* no. September, 2016.
[8] M. Hashish, "A Modeling Study of Metal Cutting With Abrasive Waterjets," *J. Eng. Mater. Technol.*, vol. 106, no. 1, p. 88, 2009.
[9] R. Manu and N. R. Babu, "An erosion-based model for abrasive waterjet turning of ductile materials," *Wear*, vol. 266, no. 11–12, pp. 1091–1097, 2009.
[10] D. C. Montgomery, *D esign and Analysis of Experiments Eighth Edition*. .
[11] FLIR. Flea3 1.3 MP Mono USB3 Vision (VITA 1300). [online] Available at: https://www.ptgrey.com/flea3-13-mp-mono-usb3-vision-vita-1300-camera [Accessed 20 Sep. 2018].